Electron microscopic observations of Rb particles and pitting in ^{129}Xe spin-exchange optical pumping cells

C. Flower,[1,a)] M. S. Freeman,[1,2,b)] M. Plue,[3] and B. Driehuys[1,c)]
[1]*Center for In Vivo Microscopy, Department of Radiology, Duke University, 311 Research Dr, Durham, North Carolina 27710, USA*
[2]*Medical Physics Graduate Program, Duke University, 2424 Erwin Rd., Ste. 101, Durham, North Carolina 27710, USA*
[3]*Shared Materials Instrumentation Facility, Duke University, 101 Science Dr., Durham, North Carolina 27710, USA*

(Received 9 January 2017; accepted 7 June 2017; published online 11 July 2017)

High-volume production of hyperpolarized ^{129}Xe by spin-exchange optical pumping (SEOP) has historically fallen short of theoretical predictions. Recently, this shortfall was proposed to be caused by the formation of alkali metal clusters during optical pumping. However, this hypothesis has yet to be verified experimentally. Here, we seek to detect the presence of alkali particles using a combination of both transmission (TEM) and scanning (SEM) electron microscopy. From TEM studies, we observe the presence of particles exhibiting sizes ranging from approximately 0.2 to 1 μm and present at densities of order 10 s of particles per 100 square microns. Particle formation was more closely associated with extensive cell usage history than short-term ($\approx$1 h) SEOP exposure. From the SEM studies, we observe pits on the cell surface. These pits are remarkably smooth, were frequently found adjacent to Rb particles, and located predominantly on the front face of the cells; they range in size from 1 to 5 μm. Together, these findings suggest that Rb particles do form during the SEOP process and at times can impart sufficient energy to locally alter the Pyrex surface. *Published by AIP Publishing*. [http://dx.doi.org/10.1063/1.4991642]

I. INTRODUCTION

Hyperpolarized (HP) noble gases have been widely applied to fields, including testing fundamental symmetries,[1] investigating surfaces and materials,[2] studying cells and biomolecules,[3] novel biosensing,[4] and functional magnetic resonance imaging (MRI) of the lung and other organs.[5] Recently, limitations in ^{3}He supply have driven a transition towards using ^{129}Xe for clinical MRI.[6] However, this application requires both high polarization levels and high throughput in order to meet the rigorous scheduling demands of a clinical setting.[7]

^{129}Xe is most efficiently polarized using spin-exchange optical pumping (SEOP).[9] By this process, the valence electrons of an alkali metal (commonly rubidium) are spin-polarized by the selective absorption of angular momentum from circularly polarized, D1-resonant photons. The polarized Rb atoms then collisionally impart their spin angular momentum to the ^{129}Xe nuclei. In addition to atomic Rb vapor and Xe gas, the SEOP environment typically contains ^{4}He gas to pressure-broaden the alkali D1 absorption cross-section and N_2 gas to efficiently quench the emission of photons that would otherwise be emitted by excited-state Rb atoms with random helicity.[10] A typical polarizer seeks to maximize polarization and throughput by using a high-power laser tuned to the 795-nm Rb D1 resonance, while a mixture lean in xenon flows continuously through the SEOP cell. Under these conditions, high alkali number density enables rapid collisional spin exchange to ^{129}Xe, which is subsequently extracted from the He and N_2 buffer gases cryogenically.[11]

Theoretically, the rate at which polarized photons are converted to ^{129}Xe nuclear spins is described by the photon efficiency. This metric is defined as the fraction of absorbed photons that are successfully converted into ^{129}Xe nuclear spins and was recently calculated for the common binary and short molecular lifetime regime by Norquay *et al.* to be 3.9%.[12] This suggests that every watt of laser light absorbed in the SEOP cell should produce $\approx$21 standard mL h^{-1} of polarized ^{129}Xe. Thus, to polarize volumes of order liters/hour, one needs to use laser powers of order 100 W. In combination with lean Xe mixtures, the theory predicts this production rate should be attained with polarizations exceeding 70%–80%. However, with the exception of some outlying, very high polarizations reported in static cells operating at low laser absorption (and thus, slow production rate),[13,14] most SEOP systems fall short of theoretically predicted performance by a factor of 2–4 when larger amounts of light are absorbed in efforts to accelerate production.

The under-performance of flow-through ^{129}Xe polarizers was recently characterized and compared to the predictions of a basic theoretical SEOP model.[15] To explain the observed discrepancy in both ^{129}Xe polarization and production rate across a broad range of optical pumping conditions, it was proposed that activated nanoscale Rb clusters, such as those described by Atutov *et al.*,[16] formed during high-power SEOP and undermined the efficiency of the process. These clusters were postulated to form in proportion to excited-state Rb density and to adversely affect SEOP by

[a)]Presently at Department of Physics, University of Maryland, College Park, Maryland 20740, USA.
[b)]Presently at Los Alamos National Laboratories, Los Alamos, New Mexico 87545, USA.
[c)]Electronic mail: bastiaan.driehuys@duke.edu

TABLE I. Cells used for the TEM study, their history, and associated observations. Cells had either a very long SEOP history or were constructed for the purpose of this study. Some cells from both categories were selected to act as control cells and were not illuminated with the laser. Cells contained a variety of features that were broadly categorized as either "particles" or "amorphous Rb features." "Particles" were persistent, roughly spherical features. "Amorphous Rb features" were either non-spherical or had a transient morphology. Some of these "amorphous Rb features" appeared to evaporate during illumination by the electron beam. The complete image data derived from each sample is available for inspection at the Harvard DataVerse.[8]

Cell ID	SEOP history (h)	Laser status during testing	Observations and characteristic sizes	Other features
A	>100	On	Particles: 200–1000 nm	
B	>100	On	Particles: 200–500 nm	Particle distribution sparser than A
C	>100	Off	Particles: 200-1000 nm Amorphous Rb features: 10–100 nm	Amorphous Rb features evaporated after exposure to TEM beam
D	0	On	No particles: N/A amorphous Rb features: 500–5000 nm	Continuous Rb background
E	0	Off	No particles: N/A amorphous Rb features: 200–500 nm	Amorphous Rb features evaporated after exposure to TEM beam

increasing Rb spin destruction, enhancing ^{129}Xe spin relaxation, and causing wasteful scattering of incident optical pumping laser light. When the effects of such hypothetical clusters were incorporated into the SEOP model, the predicted performance metrics agreed to a remarkable extent with experimental results. Although this approach successfully brought modeling and experiment into agreement, clusters had not yet been directly observed by experiment.

Here, we seek to address this gap by directly searching for such clusters and their effects on cell surfaces *ex situ*, using a combination of transmission (TEM) and scanning (SEM) electron microscopies.

II. METHODS

A total of ten standard 300 cc SEOP cells containing ≈1 g of Rb were evenly divided for TEM and SEM studies. In the TEM study, two cells served as controls and underwent the standard flow-through procedure used during hyperpolarization, without being illuminated by the laser, and thus without optical pumping. Aside from this difference, all cells were exposed to the same SEOP environmental parameters: the gas mixture was 1% Xe, 10% N_2, and 89% He; the typical pressure was ≈6 atm; the typical flow rate was ≈1.7 SLM; and the typical oven temperature was ≈150 °C as measured on the exterior glass surface of the cell. All other cells were illuminated with approximately 90 W of laser light, spectrally narrowed to ≈0.3 nm FWHM and tuned to 795 nm, the Rb D1 transition.

The characteristics of the five cells used for TEM studies are listed in Table I. This group of cells consisted of 3 heavily used (A, B, and C) and 2 new (D and E) cells. Each underwent the flow-through hyperpolarization procedure with the laser either on or off, as described in Table I. Used cells had a previous service life of greater than 100 h of SEOP. In each cell, one or more Formvar-coated TEM grids with a 200 mesh (Electron Microscopy Science-FCF200-CU-TB) were inserted via the outlet tube of the cell. During insertion, a flow of ultra-high purity (UHP) nitrogen was maintained through the cell to prevent contamination. The constant nitrogen flow, although not delivered in a glove box, was directed through the cell outlet (into which the grids were placed) and maintained throughout to prevent any atmospheric contaminants from entering the cell. Grids were placed as close as possible to the front face of the cell and away from macroscopic puddles of rubidium located near the center of the cell body. With this placement, the grids were expected to be illuminated during the subsequent SEOP process.

After grid insertion, each cell was installed in the polarizer and run under standard flow-polarization conditions, with the laser either on or off, for 1–1.5 h, the typical time to collect a 1-l batch of ^{129}Xe. Subsequently, the cell was cooled to room temperature, sealed, removed from the polarizer, and transported to the TEM for analysis. Each cell was placed in a glove bag that had one opening attached to the sample exchange of the TEM. The glove bag was purged with UHP N_2 for 5 min prior to, and continuously during extraction and sample loading. The cells were cracked open by hammer blow, and a grid was extracted and inserted into the TEM sample chamber where they were imaged at ≈10^{-8} Torr. The approximate locations from which grid samples were collected in the SEOP cell are shown in Fig. 1.

The five cells used in the SEM study all had a service life of greater than 100 h; their characteristics are summarized in Table II. Two cells (F and G) were prepared by first reacting the bulk rubidium using sequential exposure to isopropanol, ethanol, and then deionized water; no effort was

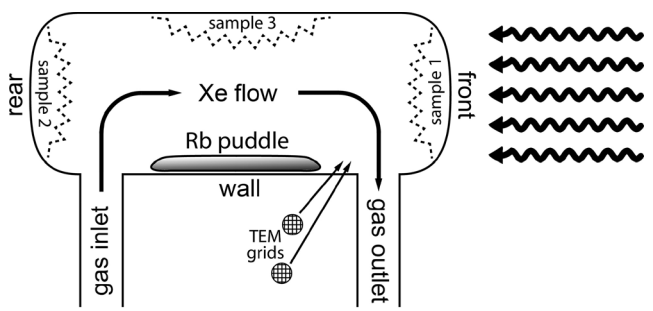

FIG. 1. Diagram of a typical SEOP cell used for SEM and TEM studies. This shows the relative locations from which each sample was taken for SEM studies and the location of the TEM grids. For SEM studies, samples were taken from the front face (sample 1), rear face (sample 2), and the sidewalls (sample 3). TEM grids were laid on the sidewall near the gas outlet at the front of the cell. In all studies, the gas flowed from the rear to the front of the cell.

TABLE II. Cells used for the SEM study, preparation details, and observations. All cells had long SEOP service histories. Cells were prepared for the SEM using several different techniques in an effort to ascertain the origin of the pits. Energy-dispersive X-ray spectroscopy (EDS) was used on some samples to determine chemical composition. The complete image data derived from all samples is available for inspection at the Harvard DataVerse.[8]

Cell ID	SEOP history (h)	Preparation	Sample location	Observations	EDS
F	>100	Alcohol and Water Rinse	Front	Particles and pits	Particles contain Rb
			Side	No particles no pits	*Not tested*
			Rear	No particles no pits	*Not tested*
G	>400	Alcohol and Water Rinse	Front	Particles and pits	Pits contain No Rb
			Side	No particles pits	*Not tested*
H	>100	No Rinse; Heat Gun on Areas of Interest	Front	Particles no pits background layer	Background layer contains Rb
			Side	Background layer	*Not tested*
I	>100	No Rinse	Front	Particles no pits background layer	Background layer contains Rb
J	>100	No Rinse	Front	Particles uncertain pits background layer	*Not tested*
			Side	No particles uncertain pits background layer	*Not tested*

made to limit their exposure to air. The other three cells (H, I, and J) were not rinsed and were maintained under nitrogen during all aspects of sample preparation. Cell H was exposed to a heat gun for ≈5 min in an effort to chase off both bulk and microscopic rubidium layers from the interior of the front face and side wall. All cells were marked on the exterior surface to aid in the subsequent identification of samples originating from the front, sidewall, and rear faces. The cells were typically broken apart by first being scored and then struck with a hammer. Pieces from these three different parts of the cell were selected for examination. For all Pyrex fragments, the side that had been interior to the cell was coated in ≈4 nm of gold using a Denton Desk IV vacuum sputter coater (Denton Vacuum, LLC, Moorestown, NJ), which is required of all non-conducting SEM samples. Samples were scanned using an FEI XL30 SEM (FEI, Inc., Hillsboro, OR).

III. RESULTS

The TEM studies on grids extracted from the used cells run with laser-on SEOP (A and B) revealed an abundant and relatively uniform distribution of particles. Examples of these particles (cell A) are seen in Fig. 2 at a variety of magnifications. Particles ranged in size from 200 nm to 1 μm in diameter and were present at a density of 20 to 30 particles per 100 square microns or $(25\pm5)\times10^6$ particles per square centimeter. Their size is somewhat larger than the proposed size of 40–600 nm used in prior modeling.[15] By contrast, the grid extracted from the never-used cell (E) run under SEOP conditions without laser exposure showed no evidence of particles. It did, however, exhibit what appeared to be diffusely distributed amorphous Rb features that evaporated under prolonged exposure to the TEM electron beam. Interestingly, the heavily used cell (C) that was run with laser-off SEOP, nonetheless exhibited evidence of particles.

SEM images taken from various locations in SEOP cells allowed for examination of the potential effects of particles on the cell surfaces. Images of the samples obtained from the front face of each cell were dominated by what appear to be circular indentations or pits. To verify that the pits were, in fact, indentations, images were taken at various tilt angles to improve depth perception. The pits were often found in large patches, with widely varying distances between them, ranging from 1 to 15 μm. Most pits appeared to have a diameter of 1–5 μm.

As seen in Fig. 3, SEM images acquired on side-wall samples of the cell F yielded no significant structure, other than what appeared to be sites of residual precipitate from

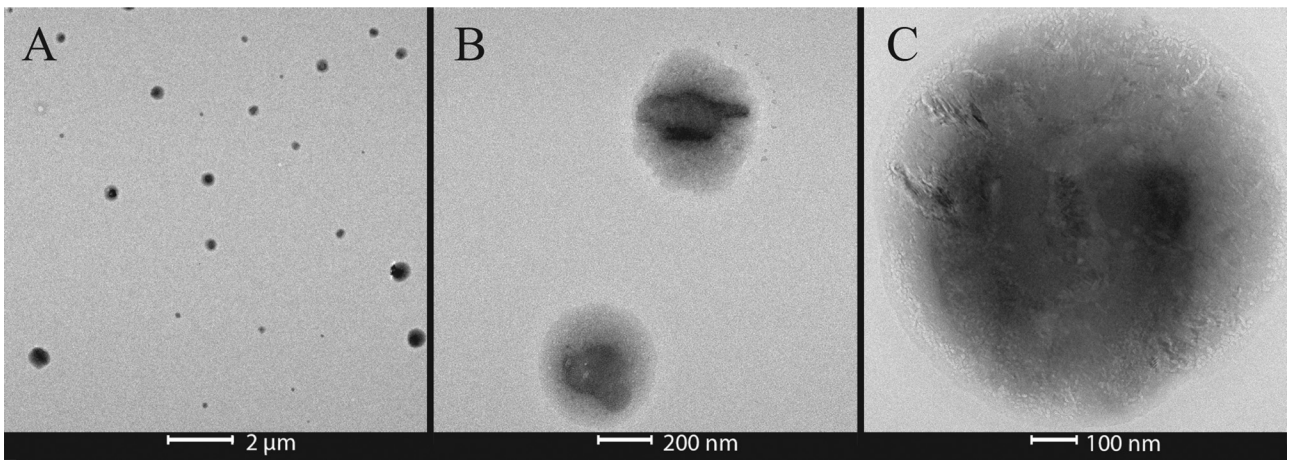

FIG. 2. TEM images at various magnifications of particles collected on a grid extracted from cell A.[8] Image A shows an overview of the relative density of the particles, ≈0.2/μm^2. Images B and C (with image C approaching maximum achievable TEM resolution) show that particles have a size of order 100 nm. These images also suggest that the particles are not uniform, as evidenced by variations in their mass density.

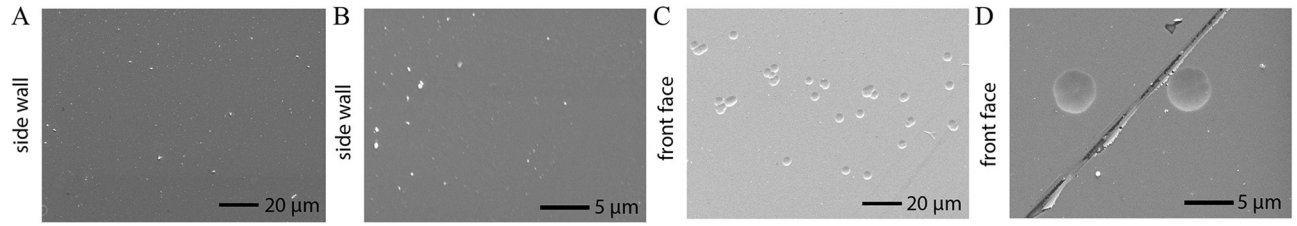

FIG. 3. SEM images from the front face and sidewall of cell F at 2000-, and 8000-× magnification.[8] Compared to the sidewall (images A and B), the front face (images C and D) of the cell shows markedly different structure dominated by pits and some Rb particles (not pictured here). Similar images of the rear face show it also to be largely devoid of features and absence of any sort of pitting.

the solvent evaporation. Similarly, images taken from samples of the rear face revealed no pitting.

Figure 4 illustrates that despite thorough rinsing, pits were often accompanied by the presence of a number of large particles. Particularly striking is their large $\approx 10\,\mu$m diameter compared to the tens to hundreds of nanometers previously postulated.[15,17] We hypothesize that this is the result of the particles having been exposed to both water and air prior to SEM. Given the hygroscopic and reactive nature of alkali metals, such exposure likely caused significant enlargement compared to their native state in an SEOP cell. As with the pits, particles were only found on samples from the front face of the cell, less frequently on the sidewall, and never on the rear face of the cell.

The elemental analysis was performed on the particles using the energy-dispersive X-ray spectroscope (EDS) on the SEM. This revealed a characteristic peak at 13.4 keV, arising from the K_α line of rubidium, as can be seen in Fig. 5. It is worth noting that no such peak could be detected in cluster-free portions of the sample, including those containing only pits.

A second cell (G) examined, as described, yielded similar results—particles and pitting on the front face and a pristine rear face. However, in this cell, some pitting was also observed on the side wall near the front face. Notably, this heavily used cell also exhibited significant cracking in between pits. To confirm that these pits and cracks were indeed in the glass itself, and not a layer of residual rubidium, EDS was performed. This revealed no characteristic peaks attributable to rubidium. To test whether particles observed on SEM were simply the result of a reaction during the cell rinsing process rather than the SEOP conditions, we also examined samples from cells (H, I, and J) that were not rinsed but were meticulously maintained under UHP N_2 during sample preparation. These trials showed a mix of particles and indentations as described in Sec. II. To better understand the nature of the surface seen in these trials, EDS was conducted and indeed revealed intense rubidium signatures. This appears to suggest that in unrinsed samples, the surface of the sample contains significant residual layers of condensed rubidium metal.

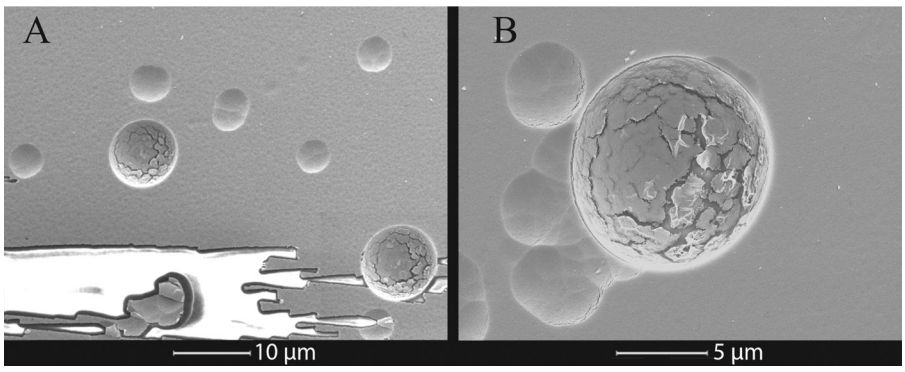

FIG. 4. SEM images of micron-scale rubidium particles adjacent to pitting on cell F.[8] These particles may have absorbed and reacted with water during the cleaning process and, thus, expanded to their 1–10 μm diameter size.

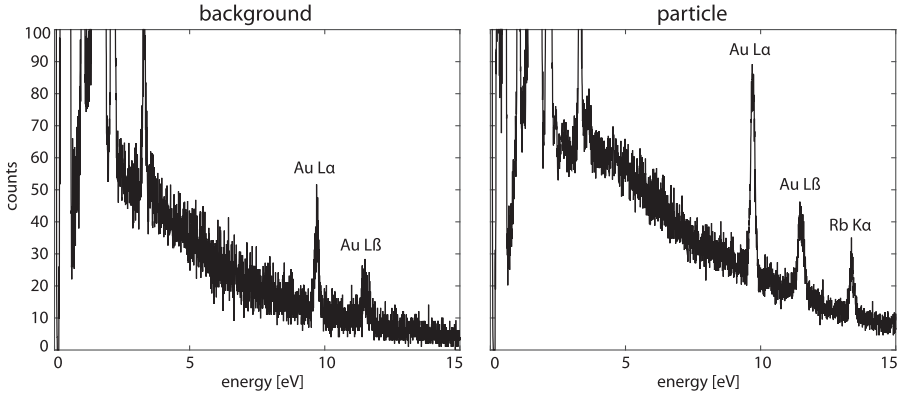

FIG. 5. EDS spectra of a particle detected via SEM, compared with the background signal from the same sample. The indicated gold peaks arise from the sputter coating used to improve sample conductivity. The majority of the background appears to be from the borosilicate glass of the cell. The particles exhibited a characteristic 13.4 keV peak, known to arise from the K_α line of rubidium.

IV. DISCUSSION

The TEM study showed two concrete observations relating to the presence of Rb particles. First, if a cell had been previously used, particles were present on the TEM grid, regardless of whether the cell had undergone laser-exposure with the grid in place. Second, in pristine, new cells, no particles were seen on TEM, regardless of whether there had been laser-exposure with the grid in place. This would seem to support the notion that particle formation does require some aspect of the SEOP conditions, albeit on a timescale longer than 1–1.5 h. Additionally, in heavily used cells that underwent SEOP without laser exposure when grids were in place, particles were still observed. This suggests that particles were already present in the cell, and therefore may persist on relatively long timescales. It is thus possible that cluster formation is mediated by some factor that is present in cells after some time, such as a contaminant (e.g., hydrogen) to aid nucleation.[18] Such factors likely increase over the course of cell usage as such cells are typically exposed to 100 liters of gas for each liter of polarized xenon they produce. It should be noted that while cell polarization performance does tend to deteriorate slightly over many hundreds of hours of use (cell T1 times decrease from 1 to 2 h to 10–15 min), polarization is certainly not dramatically better in its first hours of use. One important caveat to these interpretations is that the location of TEM grids in the cell is only roughly controllable, and the absence of particles on a single grid does not definitively rule out their presence in the cell as a whole.

The most striking finding on SEM was the presence of pits from samples originating from the front faces of cells and regions close to the front. The fact that pits were found near the front, and not the rear of the cell suggests that they cannot be explained alone by reactions associated with rinsing the cell. If pitting were caused by a chemical reaction during the cleaning of the cell, the pits would be homogeneously distributed on all cell faces. The lack of such homogeneity makes clear that pitting is a phenomenon occurring primarily at the front of the cell.

It is tempting to explain the pitting to be caused by ballistic impacts from the particles present during the SEOP process. However, it should be noted that the area around most pits is remarkably smooth. By contrast, impact craters would likely display radial fractures.[19] Thus, direct impact is likely not the cause of pitting we observe. It is conceivable that such pitting could be caused by laser ablation, mediated by impurities in the glass. This could be discerned by a control study illuminating a cell containing no rubidium. However, it is likely that the process is mediated by the rubidium itself.

We can gain further insights into the formation process by estimating the energy required to etch a hemispherical pit of radius R. Ignoring latent heat, this requires heating a volume of Pyrex glass $\frac{2R^3}{3}$ from the typical surface temperature of 150 °C to its melting point of 820 °C. Hence, forming the pit requires an energy of roughly

$$E = \frac{2\pi}{3}\rho R^3 C_m \Delta T, \tag{1}$$

where ρ is the glass density, C_m is its heat capacity, and ΔT is the temperature rise. For a pit of 1 μm radius, we estimate requiring $\approx 3 \times 10^{-12}$ J. To put this in perspective, the thermal kinetic energy of particles in a system at 425 K is closer to 10^{-20} J. Hence, the energy required to create such pits is more than 8 orders of magnitude greater than the energy thermally available to particles in the system.

The most obvious source of continuous, excess energy available to the system is provided by the optical pumping laser. In our typical SEOP cell, the 90 W optical pumping laser generates a photon flux of 1.6×10^{19} cm^{-2} s^{-1}. Such a flux would ensure that a particle 1 μm in diameter would be exposed to roughly 10^{11} photons per second. With each photon carrying 2.5×10^{-19} J of energy, this has the potential to deposit of order 10^{-8} J s^{-1} into a particle. Given the $\approx$90% reflectivity of bulk Rb at 795 nm, an estimate of 1%–10% absorption is reasonable.[20] Thus, even if $<$10% of these photons are absorbed, sufficient energy to create a pit could be imparted to a cluster in less than 1 s. Absorption of photons will heat the particle to the point of instability as suggested by simulations performed by Li *et al.*[21] In these studies, it was found that small particles ($N \approx 120$) can reach temperatures up to 800 K before undergoing fission. Thus, a picture is emerging that Rb particles are deriving energy from the pumping laser and deploying that energy to produce pits in the surface. Similar cases of rapid heating of rubidium clusters via laser irradiation have been reported.[16] Although we cannot definitively claim this to be the mechanism responsible, it may explain why pits appear to be relatively sparse and are primarily found near the front face of the cell. It is here that the laser beam enters the cell with highest intensity.

V. CONCLUSION

The ability to image the interior surface of SEOP cells has provided information on complex surface interactions that have never previously been considered in the performance of high-volume SEOP polarizers. The observation of condensed and persistent rubidium particles in both TEM and SEM images suggests that the rubidium is forming compounds either on the surface of the glass or in the gas stream. However, the *ex situ* detection of particles containing Rb does not definitively implicate their presence or formation during SEOP, nor inform the postulated effects on the polarization process. That being said, the SEM observation that particles and their potentially associated pitting were often co-localized suggests that the pits could have been formed by the particles themselves. Although it appears clear that over time the SEOP process promotes the formation of Rb aggregates larger than an atom, it does not appear to do so instantaneously. The preference for pitting near the front of the cell does support the notion that these mechanisms of particle formation and destruction are most active in the regions of highest laser intensity (we note that this association could be strengthened by a study in which the gas flow direction was reversed). This suggests that there is likely a useful limit on the productive deployment of additional laser power in a confined space. This may explain the success of ^{129}Xe polarizer systems that use larger cells[22] and/or cooler operating parameters[14] to limit overly localized absorption of laser power. Thus, future SEOP systems may be able to

regain full efficiency by using larger optical pumping cells that effectively absorb all the light from high-power lasers at moderate temperatures and alkali number densities.

ACKNOWLEDGMENTS

This study was funded by NIH/NHLBI R01HL105643 and performed in part at the Duke University Shared Materials Instrumentation Facility (SMIF), a member of the North Carolina Research Triangle Nanotechnology Network (RTNN), which was supported by the National Science Foundation (Grant No. ECCS-1542015) as part of the National Nanotechnology Coordinated Infrastructure (NNCI). Analysis was conducted with the additional support from the Duke Center for In Vivo Microscopy, an NIH/NIBIB National Biomedical Technology Resource Center (P41 EB015897).

[1]F. Allmendinger, W. Heil, S. Karpuk, W. Kilian, A. Scharth, U. Schmidt, A. Schnabel, Y. Sobolev, and K. Tullney, Phys. Rev. Lett. **112**, 110801 (2014).
[2]H. J. Jänsch, P. Gerhard, and M. Koch, PNAS **101**, 13715 (2004).
[3]D. Baumer, E. Brunner, P. Blümler, P. P. Zänker, and H. W. Spiess, Angew. Chem. Int. Ed. **45**, 7282 (2006).
[4]L. Schroder, T. J. Lowery, C. Hilty, D. E. Wemmer, and A. Pines, Science **314**, 446 (2006).
[5]R. T. Branca, T. He, L. Zhang, C. S. Floyd, M. Freeman, C. White, and A. Burant, PNAS **111**, 18001 (2014).
[6]J. P. Mugler and T. A. Altes, J. Magn. Reson. Imaging **37**, 313 (2013).
[7]M. He, S. H. Robertson, S. S. Kaushik, M. S. Freeman, R. S. Virgincar, J. Davies, J. Stiles, W. M. Foster, H. P. McAdams, and B. Driehuys, Magn. Reson. Imaging **33**, 877 (2015).
[8]C. Flower, M. Freeman, M. Plue, and B. Driehuys, *SEM and TEM Images of the Interior of Spin-Exchange Optical Pumping Cells used in ^{129}Xe Flow-Through Polarizers* (Harvard Dataverse, 2017).
[9]S. Appelt, A. B.-A. Baranga, C. J. Erickson, M. V. Romalis, A. R. Young, and W. Happer, Phys. Rev. A **58**, 1412 (1998).
[10]E. S. Hrycyshyn and L. Krause, Can. J. Phys. **48**, 2761 (1970).
[11]B. Driehuys, G. D. Cates, E. Miron, K. Sauer, D. K. Walter, and W. Happer, Appl. Phys. Lett. **69**, 1668 (1996).
[12]G. Norquay, S. R. Parnell, X. Xu, J. Parra-Robles, and J. M. Wild, J. Appl. Phys. **113**, 044908 (2013).
[13]P. Nikolaou, A. M. Coffey, M. J. Barlow, M. S. Rosen, B. M. Goodson, and E. Y. Chekmenev, Anal. Chem. **86**, 8206 (2014).
[14]P. Nikolaou, A. M. Coffey, L. L. Walkup, B. M. Gust, N. Whiting, H. Newton, S. Barcus, I. Muradyan, M. Dabaghyan, G. D. Moroz, M. S. Rosen, S. Patz, M. J. Barlow, E. Y. Chekmenev, and B. M. Goodson, PNAS **110**, 14150 (2013).
[15]M. S. Freeman, K. Emami, and B. Driehuys, Phys. Rev. A **90**, 023406 (2014).
[16]S. N. Atutov, A. I. Plekhanov, A. M. Shalagin, R. Calabrese, L. Tomassetti, and V. Guidi, Eur. Phys. J. D **66**, 140 (2012).
[17]C. Duthler, S. Johnson, and H. Broida, Phys. Rev. Lett **26**, 1236 (1971).
[18]A. Tam, G. Moe, and W. Happer, Phys. Rev. Lett. **35**, 1630 (1975).
[19]J. F. Vedder and J.-C. Mandeville, J. Geophys. Res. **79**, 3247, doi:10.1029/JB079i023p03247 (1974).
[20]N. V. Smith, Phys. Rev. B **2**, 2840 (1970).
[21]Y. Li, E. Blaisten-Barojas, and D. A. Papaconstantopoulos, Phys. Rev. B **57**, 15519 (1998).
[22]I. C. Ruset, S. Ketel, and F. W. Hersman, Phys. Rev. Lett. **96**, 053002 (2006).